Article

The Properties of Zn-Doped AlSb Thin Films Prepared by Pulsed Laser Deposition

Ping Tang [1,2,3,†], Weimin Wang [2,3,†], Bing Li [1,*], Lianghuan Feng [1] and Guanggen Zeng [1]

[1] College of Materials Science and Engineering, Sichuan University, Chengdu 610064, China; tangp@ioe.ac.cn (P.T.); lh.feng@scu.edu.cn (L.F.); zengguanggen@scu.edu.cn (G.Z.)

[2] Guangxi Key Laboratory of Automatic Detecting Technology and Instruments, Guilin University of Electronic Technology, Guilin 541004, China; wwm@ioe.ac.cn

[3] State Key Laboratory of Optical Technologies on Nano-Fabrication and Micro-Engineering, Institute of Optics and Electronics, Chinese Academy of Sciences, P.O. Box 350, Chengdu 610209, China

* Correspondence: libing@scu.edu.cn; Tel.: +86-28-8541-2542

† These authors contributed equally to this work.

check for updates

Abstract: Aluminum antimony (AlSb) is a promising photovoltaic material with a band gap of about 1.62 eV. However, AlSb is highly deliquescent and not stable, which has brought great difficulties to the applications. Based on the above situation, there are two purposes for preparing our Zn-doped AlSb (AlSb:Zn) thin films: One is to make P-type AlSb and the other is to find a way to suppress the deliquescence of AlSb. The AlSb:Zn thin films were prepared on glass substrates at different substrate temperatures by using the pulsed laser deposition (PLD) method. The structural, surface morphological, optical, and electrical properties of AlSb:Zn films were investigated. The crystallization of AlSb:Zn thin films was enhanced and the electrical resistivity decreased as the substrate temperature increased. The scanning electron microscopy (SEM) images indicated that the grain sizes became bigger as the substrate temperatures increased. The Raman vibration mode AlSb:Zn films were located at ~107 and ~142 cm^{-1} and the intensity of Raman peaks was stronger at higher substrate temperatures. In the experiment, a reduced band gap (1.4 eV) of the AlSb:Zn thin film was observed compared to the undoped AlSb films, which were more suitable for thin-film solar cells. Zn doping could reduce the deliquescent speed of AlSb thin films. The fabricated heterojunction device showed the good rectification behavior, which indicated the PN junction formation. The obvious photovoltaic effect has been observed in an FTO/ZnS/AlSb:Zn/Au device.

Keywords: AlSb:Zn films; decreased band gap; deliquescence; PN junction

1. Introduction

Aluminum antimony (AlSb) is a binary compound semiconductor material with a theoretical indirect band gap of 1.62 eV that is very compatible with the solar spectrum [1]. Due to the proper band gap and high carrier mobility, AlSb has wide applications in anode materials for Li-ion battery, PN junction diodes, transistors, room temperature radiation detection, room temperature gamma ray detection, photovoltaic conversion devices, and so on [2–4]. As a potential absorption material, the theoretical photoelectric conversion efficiency of AlSb based solar cells is up to 27%, which has recently drawn extensive attention [5,6].

It is well known that some methods have been used to prepare AlSb, such as bulk AlSb crystals that were prepared by the Czochralski method [7,8]. AlSb thin films were deposited by sputtering [9], evaporation [10], electrodeposition [4], hot wall epitaxy [11], molecular beam epitaxy (MBE) [2,12], metal organic chemical vapor deposition (MOCVD) [13], and pulsed laser deposition (PLD) [14].

Previously we have successfully prepared AlSb thin films based on our facile PLD method [15]. However, Al and Sb ions can easily react with air and moisture. Recently, theoretical calculations predict Zn doping can dramatically increase the chemical stability and reduce the band gap for AlSb thin films [16]. Meanwhile, experimental element doping of AlSb while the thin film is formed is still in its infancy. In this paper, we demonstrated the preparation of Zn-doped AlSb thin films by the one-step facile PLD method. The optical and electrical properties of the films have been studied. An AlSb-based photovoltaic device was fabricated, from which we observed an obvious photovoltaic effect.

2. Experimental

A KrF excimer laser (Lambda Physik Compex 201, Dieburg, Germany, λ = 248 nm, pulse duration = 20 ns) was employed to fabricate AlSb:Zn thin films on glass substrates by the PLD method. A pulse energy of 110 mJ with a laser repetition rate of 6 Hz was pulsed on a single source of AlSb target. This was mixed with 0.1 at.% Zinc (purity 99.99% atomic percentage) and used to grow AlSb:Zn thin films. The background vacuum was set as lower than 1.5×10^{-3} Pa (the ultimate vacuum of the PLD system) during the entire deposition process. For the very low deposition rate at higher deposition pressure, the lowest vacuum in the experiment was necessary. The films with few pinholes were obtained under these parameters. During the growth, the glass substrates were kept hot, so the substrate temperatures varied in the range of 300 °C to 400 °C. The films were amorphous below 300 °C and it was difficult to prepare AlSb:Zn films above 400 °C due to re-evaporation in the PLD system. Finally, all the samples naturally cooled down to room temperature in the vacuum chamber. The thickness of AlSb:Zn thin films was about 400 nm.

The optical transmittance of AlSb:Zn thin films was measured by ultraviolet-visible spectroscopy (Perkin Elmer Lambda 950, Waltham, MA, USA). The X-ray diffraction (XRD) spectra for structure analysis were measured by DanDong Hao Yuan DX-2700, Dandong, China, using Cu Kα radiation (λ = 1.5405 Å). The film thickness was examined by a probe surface profiler (Ambios Technology XP-2, Santa Cruz, CA, USA). The scanning electron microscopy (SEM) images of AlSb:Zn thin films were obtained by HITACHI S5200 (Tokyo, Japan). A Labram HR Evolution Raman spectrometer (Horiba, Kyoto, Japan) with a 532 nm Argon laser was used to characterize the Raman spectra of the films. The valence band spectrum was carried out by using an X-ray photoelectron spectrometer (XPS, THERMO FISHER ESCALAB-250Xi, Waltham, MA, USA).

Based on the above studies, the FTO/ZnS/AlSb:Zn/Au device was fabricated and an obvious photovoltaic effect was observed in the device. Figure 1 depicts the structure of an AlSb-based solar cell, in which both the ZnS thin film (~200 nm) and the AlSb:Zn thin film (~1 μm) were deposited by the PLD method. The Au electrode (~100 nm) was prepared by vacuum evaporation. The ZnS thin film was deposited at the substrate temperature of 200 °C by the PLD method [17,18]. A pulse energy of 110 mJ with a laser repetition rate of 6 Hz was applied for the growth of the ZnS thin films. The distance between the target and the substrate was 4 cm. The deposition rate of ZnS was 15 nm/min. As an absorber layer, the AlSb:Zn thin film should be thicker than the 400 nm of the thin film samples. The FTO was the commercial SnO_2:F thin film (~500 nm), with a sheet resistance of 15 Ω/□. The area of the unit cell was 0.0707 cm^2. The open circuit voltage was measured by a multimeter under an AM 1.5 illumination at room temperature.
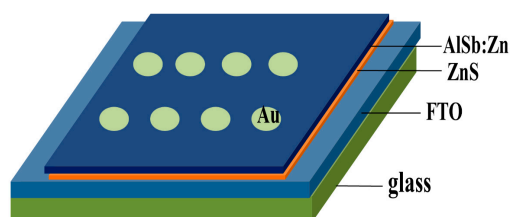
Figure 1. Structure of AlSb-based solar cells.

3. Results and Discussion

The full scale XRD patterns of AlSb:Zn thin films deposited at different temperatures are shown in Figure 2a. There were two or more diffraction peaks with cubic structure for all the AlSb:Zn films, indicating that all the films were polycrystalline. Two space groups, F43m and P3a, of AlSb are observed in Figure 2a. Polycrystalline AlSb:Zn films exhibited a preferred (200) orientation of space group F43m. At lower substrate temperatures, there was (200) plane of space group F43m and (200), (311), and (400) planes of space group Pa3. However, another diffraction peak of (400) plane of space group F43m was observed at 400 °C. Meanwhile, the intensity of main diffraction peak increased sharply as the substrate temperature increased from 300 °C to 400 °C, which indicated that the crystallization of the AlSb:Zn thin film was enhanced when the substrate temperatures were elevated. High substrate temperature is very important for obtaining crystal AlSb:Zn films during the whole deposition process. The higher substrate temperature may help the growing species to obtain a higher mobility. Therefore it may promote the lateral growth of the AlSb:Zn thin films.
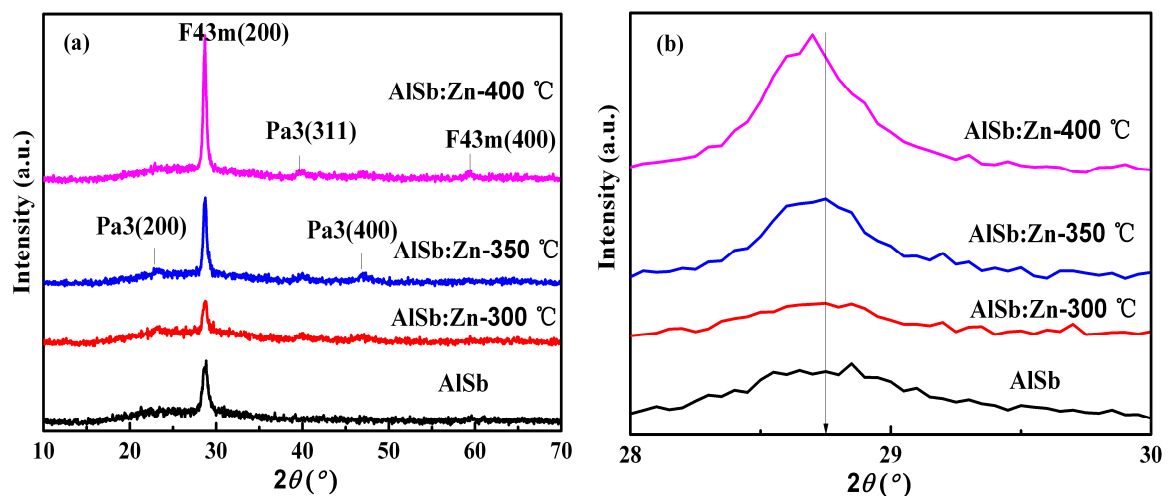
Figure 2. (**a**) Full scale and (**b**) enlarged scale XRD patterns of AlSb:Zn thin films deposited at different substrate temperatures.

Figure 2 shows the enlarged scale (28°–30°) of the XRD patterns. Compared with the XRD of undoped AlSb film, the diffraction peaks of all the AlSb:Zn films had a little left shift. Due to the Zn doping in AlSb:Zn structure, Zn atoms would substitute Al atoms resulting excess holes. AlSb films doped Zn were P-type materials. Due to differences in atomic radius sizes of Al and Zn atoms, the residual strain of the films was originated from atomic size differences, thus the diffraction peak had a shift for Zn-doping.

The surface morphology properties are very important for solar cells and other devices because of their effect on the interface among different film layers. The SEM images of AlSb:Zn thin films were shown in Figure 3. Obvious grains were observed at the higher substrate temperatures (350 and 400 °C) while no grains could be seen at the lower substrate temperature (300 °C), which was in accordance with the XRD results. Moreover, as the substrate temperature increased, the grain sizes became bigger. When the substrate temperature reached 400 °C, the smallest grain sizes were ~20 nm and the biggest grain sizes were ~100 nm by using the scale bar. The big grain size was helpful for the carrier transportation in AlSb-based solar cells.
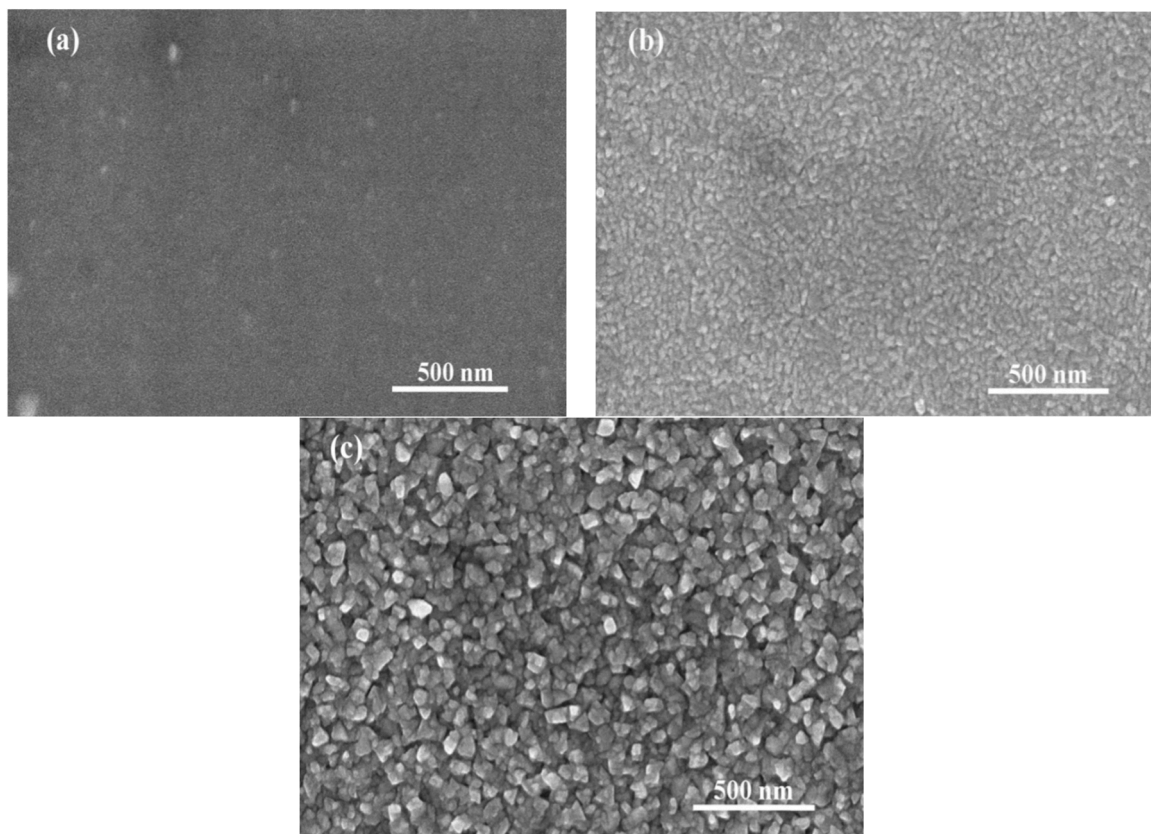
Figure 3. SEM images of AlSb:Zn thin films deposited at different substrate temperatures: (**a**) 300 °C; (**b**) 350 °C; (**c**) 400 °C.

Figure 4 showed the Raman spectra of AlSb:Zn thin films recorded in the wide range of 50–230 cm^{-1}. The Raman profiles of all the AlSb:Zn thin films were similar and the Raman peaks appeared in the same position located at ~107 and ~142 cm^{-1}, which revealed similar variations existing in the AlSb:Zn thin film structures. The intensity of the Raman peaks improved as the substrate temperature increased from 300 °C to 400 °C. The improved intensity of the Raman spectra could be attributed to the increased crystallinity of the films. The scattering energy consumption was larger for the poor crystallinity and made the intensity of Raman peak decrease. The dominated Raman peak was at ~142 cm^{-1}, which was close to the LO peak for bulk AlSb (~150 cm^{-1}). It can be noted that one peak observed, located at ~107 cm^{-1}, was similar to the Raman spectra of AlSb thin films deposited by the PLD method by Das et al. [14]. Compared with the AlSb thin films, the Raman peak positions had a left shift. It is known that the shift of Raman peaks can be attributed to residual stress, structural disorder, doping, and crystal defect in the films. When Zn atoms substituted Al atoms, the crystal lattice of AlSb would have changed for the different atomic radius sizes of Al and Zn atoms, causing the AlSb crystal lattice to be distorted. Thus, the crystal lattice distortion appeared as a shift in Raman spectrum [19,20]. Approximately the same Raman shift indicated similar structural stress among the three AlSb:Zn thin films [21]. Meanwhile, the same Raman shift peaks revealed similar structures among the AlSb:Zn thin films.

The electrical resistivity of AlSb:Zn thin films is shown in Figure 5. The electrical resistivity of the AlSb:Zn thin films gradually decreased from 7.5×10^{-2} to 4.3×10^{-2} Ω·cm as the substrate temperature increased. The electrical resistivity of the AlSb:Zn thin films was lower at the higher substrate temperature for the bigger grain size, reducing the grain boundary scattering.
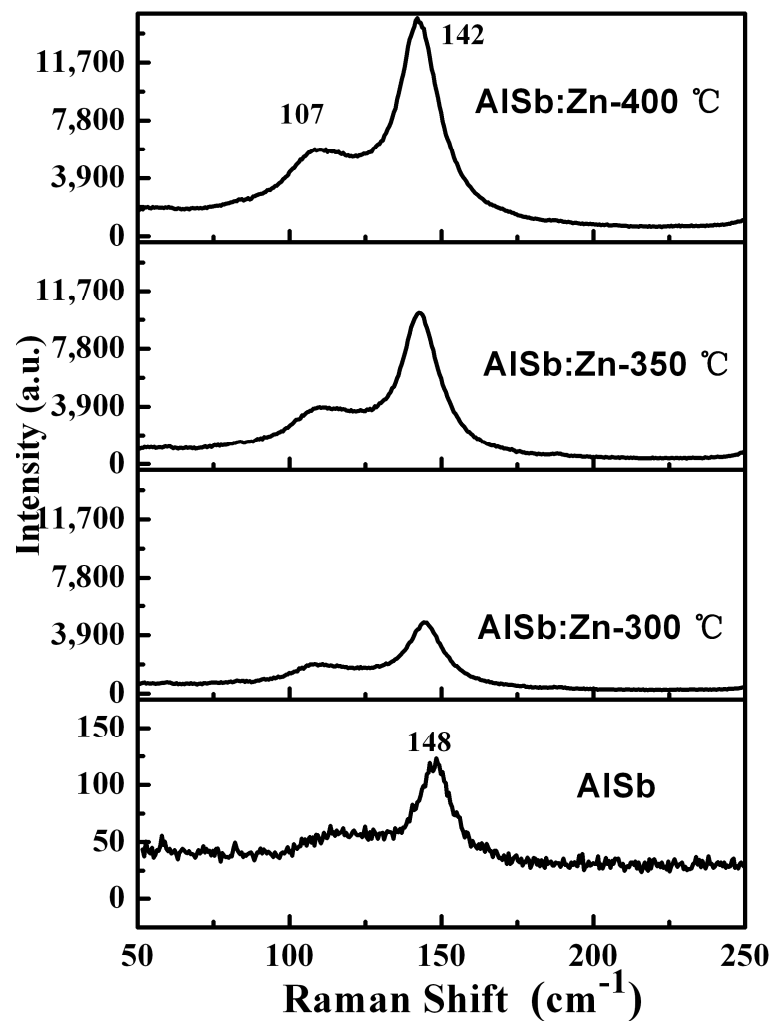
Figure 4. Raman spectra of AlSb:Zn thin films deposited at different substrate temperatures.
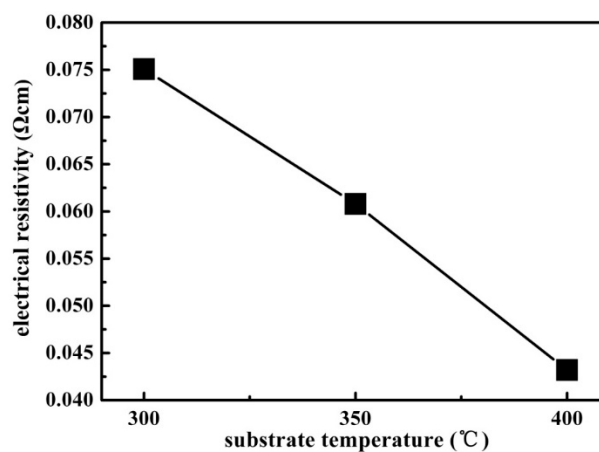
Figure 5. The electrical resistivity of AlSb:Zn thin films deposited at different substrate temperature.

The optical transmittance spectra of all the AlSb:Zn thin films were obtained by ultraviolet-visible spectroscopy (not shown here). The absorption coefficient α can be calculated from the transmittance spectra. The indirect band gap material is subject to the following relationship [11]:

$$\alpha h\nu = A(h\nu - E_g)^2 \tag{1}$$

where A is a constant, $h\nu$ is the photon energy, and E_g is the optical band gap. The plot of $(\alpha h\nu)^{1/2}$ versus $h\nu$ profile of a representative AlSb:Zn film deposited at 400 °C was given in Figure 6. The extrapolation of the straight line to $(\alpha h\nu)^{1/2} = 0$ axis gives the value of E_g. A band gap of 1.4 eV was obtained, which was lower than the theoretical band gap of AlSb. The valence band maximum of AlSb moved to the high energy zone, while the conduction band minimum moved to the lower zone for the Zn doping, thus the band gap became smaller. As a potential absorber layer of solar cells, the decreased band gap is beneficial for the light absorption in the long wavelengths.

The valence band spectrum of a representative AlSb:Zn film deposited at 400 °C was carried out by XPS. Figure 7 shows the valence band spectrum of the film. The valence band maximum was determined by an extrapolation of a line fit to the leading edge of the spectrum. The valence band maximum was −0.78 eV for the AlSb:Zn film, which means the Fermi level was below the valence band maximum and the AlSb:Zn films were P-type materials. Zn doping changed the energy band structure of AlSb.
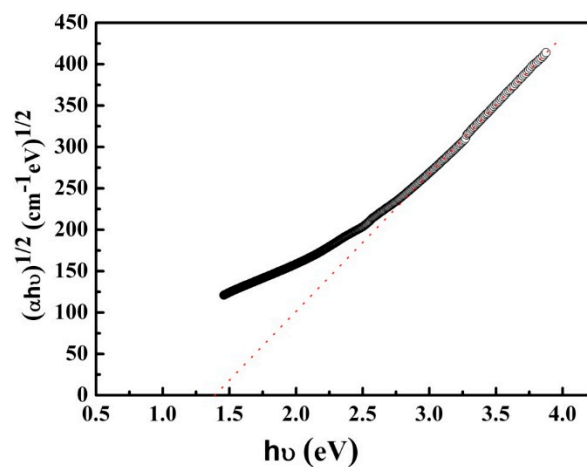
Figure 6. Plot of $(\alpha h\nu)^{1/2}$ versus $h\nu$ profile of a representative AlSb:Zn film deposited at 400 °C.
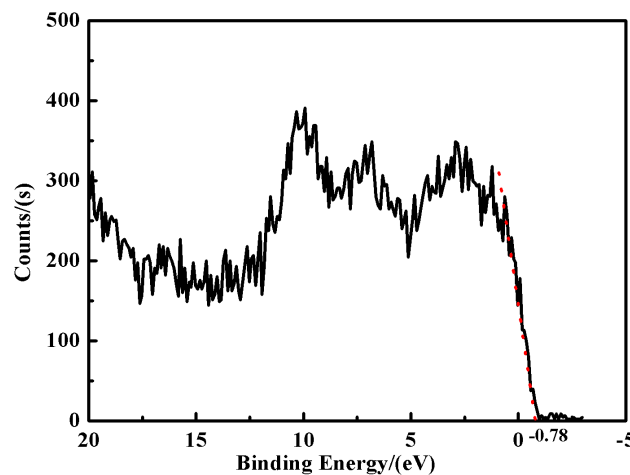
Figure 7. The valence band spectrum of a representative AlSb:Zn film deposited at 400 °C.

To compare the deliquescence of the AlSb and AlSb:Zn thin films, the films were stored in a vacuum chamber (about 2 Pa). Figure 8 shows the SEM images of the AlSb and AlSb:Zn thin films stored in the vacuum chamber for 48 h. There were some agglomerates on the surface of the films after deliquescence. In the same vacuum chamber, the quantities of agglomerate of AlSb:Zn were fewer than AlSb. It indicated that Zn doping can reduce the deliquescent speed of AlSb thin films.
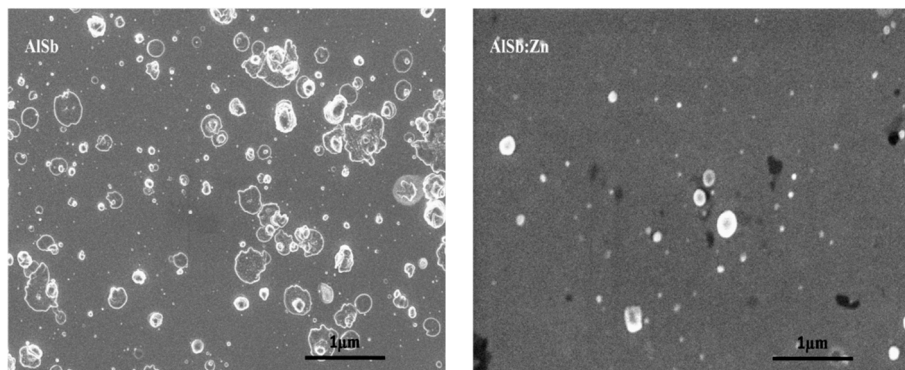
Figure 8. SEM images of AlSb and AlSb:Zn thin films stored in a vacuum chamber for 48 h.

The purpose of studying AlSb-base solar cells is to get low cost and environmental solar cells. In our previous work, ZnS/AlSb thin film solar cells were simulated by using wxAMPS and high conversion efficiency was obtained in the solar cells [15]. For the AlSb-base solar cells, ZnS is considered as one of the promising N-type buffer layer materials due to wide band gap and high transmittance [22,23]. Moreover, both of Zn and S elemental resources are abundant, low cost and environment-friendly. The PN junction is formed when ZnS films (N-type materials) are combined with AlSb:Zn films (P-type materials), as shown in Figure 9. The build-in electrical field exists at the interface of ZnS and AlSb:Zn films, which is able to drive electrons away from the interface and accelerates the collection of electrons.
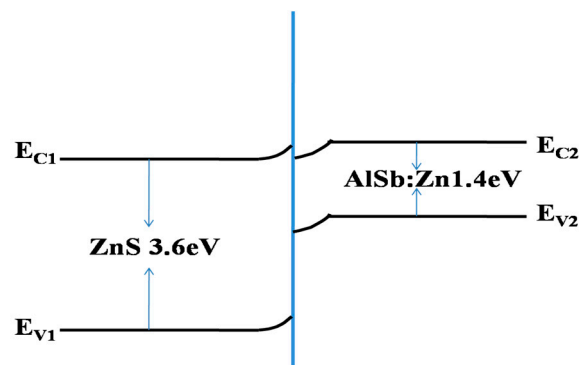
Figure 9. The energy band of the ZnS/AlSb:Zn heterojunction.

After the above studies, we fabricated AlSb-based solar cell with a structure of FTO/ZnS/AlSb:Zn/Au. AlSb:Zn thin film was deposited at the optimized condition. Over 60 mV light open circuit voltage was obtained in the AlSb:Zn-based solar cell. However, it was very difficult to obtain the light *J-V* curve because the short circuit current of the device was too small. The open circuit voltage was influenced by recombination of grain boundary, characteristics of interfaces, and carrier transportation.

The dark *I-V* curve is shown in Figure 10. The dark *I-V* curve shows the PN junction of ZnS/AlSb:Zn structure was combined. Environmental and low-cost AlSb-based PN junction diodes can be prepared by the economic PLD method. AlSb:Zn thin films are promising materials for photovoltaic and other optoelectronic devices. The values of the diode factor (*A*) and the reverse saturation current density (J_0) calculated from dark *I-V* curve were 11.6 and 15.8 mA/cm^2, respectively. The high value of *A* indicates that the defect density of the PN junction was very large and the recombination velocity of defect was high in the device [24]. The high J_0 and leakage current have an effect on the open circuit voltage of the solar cells, so the open circuit voltage is very small. Our future work should mainly focus on optimizing the structure of the AlSb-based solar cell.
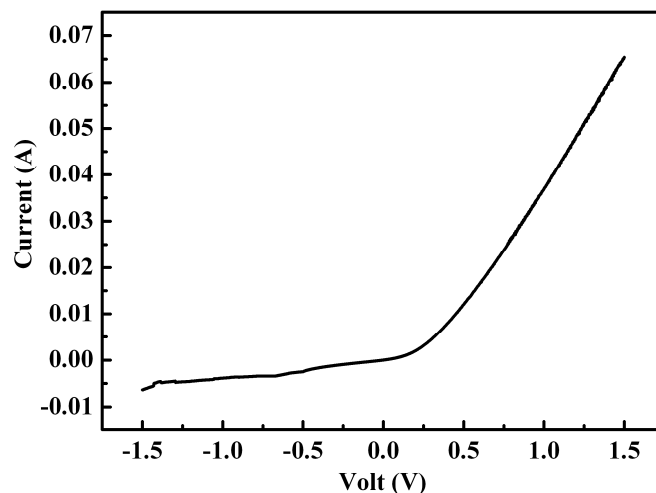
Figure 10. Dark *I-V* curve of a ZnS/AlSb:Zn thin film solar cell.

4. Conclusions

AlSb:Zn thin films were successfully deposited on glass substrates by the PLD method using a single source of AlSb:Zn target. The substrate temperatures influenced the properties of the thin films. The crystallization of AlSb:Zn thin films was improved by increasing the substrate temperature. The grain sizes became bigger with the increased substrate temperatures in the temperature range of 300 °C to 400 °C. The intensity of Raman peaks at ~107 and ~142 cm^{-1} was enhanced for higher substrate temperatures samples and the electrical resistivity decreased with the increase of the substrate temperature. At the optimized substrate temperature of 400 °C, the optical band gap of AlSb:Zn thin film was 1.4 eV. Zn doping could suppress the deliquescence of AlSb thin films. The PN junction diode of the ZnS/AlSb:Zn structure was successfully prepared by showing good PN junction characteristic. Over 60 mV light open circuit voltage was obtained in the FTO/ZnS/AlSb:Zn/Au device. These results indicate that environmental and low-cost AlSb-based PN junction diodes could be prepared by the economic PLD method and that AlSb:Zn thin films are a promising material for photovoltaic and other optoelectronic devices in future design. We believe that once this technology is widely used, AlSb-based solar cells will bring new opportunities.

Author Contributions: Writing—Original Draft Preparation, P.T.; Project Administration, B.L.; Funding Acquisition, W.W.; Formal Analysis, L.F. and G.Z.

Conflicts of Interest: The authors declare no conflict of interest.

References

1. Fischer, T.E. Reflectivity, photoelectric emission, and work function of AlSb. *Phys. Rev.* **1965**, *139*, A1228. [CrossRef]
2. Vaughan, E.I.; Addamane, S.; Shima, D.M.; Balakrishnan, G.; Hecht, A.A. High-resistivity semi-insulating AlSb on GaAs substrates grown by molecular beam epitaxy. *J. Electron. Mater.* **2016**, *45*, 2025–2030. [CrossRef]
3. Kareem, T.A.; Kaliani, A.A. X-ray diffraction study of plasma exposed and annealed AlSb bilayer thin film. *Plasma Sci. Technol.* **2013**, *15*, 382. [CrossRef]
4. Gandhi, T.; Raja, K.S.; Misra, M. Room temperature electrodeposition of aluminum antimonide compound semiconductor. *Electrochim. Acta* **2008**, *53*, 7331–7337. [CrossRef]
5. Armantrout, G.A.; Yee, J.H. AlSb as a potential photovoltaic material. In Proceedings of the 2nd Photovoltaic Solar Energy Conference, Berlin, Germany, 23–26 April 1979; pp. 960–967.

6.   He, J.; Wu, L.; Feng, L.; Zheng, J.; Zhang, J.; Li, W.; Li, B.; Cai, Y. Structural, electrical and optical properties of annealed Al/Sb multilayer films. *Sol. Energy Mater. Sol. Cells* **2011**, *95*, 369–372. [CrossRef]

7.   Herczog, A.; Haberecht, R.R.; Middleton, A.E. Preparation and properties of aluminum antimonide. *J. Electrochem. Soc.* **1958**, *105*, 533–540. [CrossRef]

8.   Allred, W.P.; Mefferd, W.L.; Willardson, R.K. The preparation and properties of aluminum antimonide. *J. Electrochem. Soc.* **1960**, *107*, 117–122. [CrossRef]

9.   Baggetto, L.; Marszewski, M.; Górka, J.; Jaroniec, M.; Veith, G.M. AlSb thin films as negative electrodes for Li-ion and Na-ion batteries. *J. Power Sources* **2013**, *243*, 699–705. [CrossRef]

10. Johnson, J.E. Aluminium antimonide thin films by coevaporation of the elements. *J. Appl. Phys.* **1965**, *36*, 3193–3195. [CrossRef]

11. Singh, T.; Bedi, R.K. Growth and properties of aluminium antimonide films produced by hot wall epitaxy on single-crystal KCl. *Thin Solid Films* **1998**, *312*, 111–115. [CrossRef]

12. Da Silva, F.W.O.; Raisin, C.; Nouaoura, M.; Lassabatere, L. Auger and electron energy loss spectroscopies study of the oxidation of AlSb (001) thin films grown by molecular beam epitaxy. *Thin Solid Films* **1991**, *200*, 33–48. [CrossRef]

13. Leroux, M.; Tromson-Carli, A.; Gibart, P.; Vérié, C.; Bernard, C.; Schouler, M.C. Growth of AlSb on insulating substrates by metal organics chemical vapour deposition. *J. Cryst. Growth* **1980**, *48*, 367–378. [CrossRef]

14. Das, S.; Ghosh, B.; Hussain, S.; Bhar, R.; Pal, A.K. Pulsed laser deposition: A viable route for the growth of aluminum antimonide film. *J. Cryst. Growth* **2015**, *419*, 12–19. [CrossRef]

15. Tang, P.; Li, B.; Feng, L.; Wu, L.; Zhang, J.; Li, W.; Zeng, G.; Wang, W.; Liu, C. Structural, electrical and optical properties of AlSb thin films deposited by pulsed laser deposition. *J. Alloy. Compd.* **2017**, *692*, 22–25. [CrossRef]

16. Bao, X.-L.; Zhang, K.-Y.; Li, C.-X.; Ran, Y.-Q. Effects of Cu and Zn doping on electronic structure and optical properties of AlSb. *J. Synth. Cryst.* **2012**, *41*, 1451–1457. (In Chinese)

17. Ming, Z.X.; Ding, C.; Li, B.; Zhang, J.Q.; Li, W.; Wu, L.L.; Feng, L.H.; Wu, J.D. Properties study of ZnS thin films fabricated at different substrate temperatures by pulsed laser deposition. *Adv. Mater. Res.* **2013**, *821–822*, 835–840. [CrossRef]

18. Yano, S.; Schroeder, R.; Ullrich, B.; Sakai, H. Absorption and photocurrent properties of thin ZnS films formed by pulsed-laser deposition on quartz. *Thin Solid Films* **2003**, *423*, 273–276. [CrossRef]

19. Cheewajaroen, K.; Saengkaew, P.; Sanorpim, S.; Yordsri, V.; Thanachayanont, C.; Nuntawong, N.; Rathanasakulthong, W. Characterization of N-type and P-type Aluminum Antimonides on Si substrates for room-temperature optoelectronic devices. *Mat. Sci. Semicond. Process.* **2018**, *88*, 224–233. [CrossRef]

20. Hao, C.; Wang, R. Raman spectrum of Zn:LiNbO$_3$ crystal. *Mat. Sci. Technol.* **2004**, *12*, 202–204. (In Chinese)

21. Yan, X.; Li, W.; Aberle, A.G.; Venkataraj, S. Investigation of the thickness effect on material and surface texturing properties of sputtered ZnO:Al films for thin-film Si solar cell applications. *Vacuum* **2016**, *123*, 151–159. [CrossRef]

22. Martínez-Martínez, S.; Mayén-Hernández, S.A.; de Moure-Flores, F.; Arenas-Arrocena, M.C.; Campos-González, E.; Zamora-Antuñano, M.A.; Arellano-Badillo, V.M.; Santos-Cruz, J. Sulfiding effects on ZnS thin films obtained by evaporation technique. *Vacuum* **2016**, *130*, 154–158. [CrossRef]

23. Chelvanathan, P.; Yusoff, Y.; Haque, F.; Akhtaruzzaman, M.; Alam, M.M.; Alothman, Z.A.; Rashid, M.J.; Sopian, K.; Amin, N. Growth and characterization of RF-sputtered ZnS thin film deposited at various substrate temperatures for photovoltaic application. *Appl. Surf. Sci.* **2015**, *334*, 138–144. [CrossRef]

24. Zhang, M.; Qiu, L.; Li, W.; Zhang, J.; Wu, L.; Feng, L. Copper doping of MoO$_x$ thin film for CdTe solar cell. *Mat. Sci. Semicond. Process.* **2018**, *86*, 49–57. [CrossRef]